

IAC-14-A6.9.1

OBSERVATION AND ANALYSIS OF THE APPARENT SPIN PERIOD VARIATIONS OF INACTIVE BOX-WING GEOSYNCHRONOUS RESIDENT SPACE OBJECTS

Mr. Michael A. Earl

Royal Military College of Canada, Canada, Michael.Earl@rmc.ca

Dr. Gregg A. Wade*

Between March 2012 and September 2014, ground-based broadband photometric observations of six inactive geosynchronous (GEO) resident space objects (RSOs) of box-wing design were performed in order to study their attitude dynamics. Each RSO was observed to have an apparent spin period that varied over time in a manner that suggested periodic behaviour. The RSOs' apparent spin periods differed from one another, ranging between 140 seconds and 1900 seconds. The apparent spin period variation features, including the amplitudes and shapes, also appeared different from one another and suggested a relationship between the average apparent spin period and the spin period variation amplitude. The observed spin period variations suggested that one or more disturbance torques were acting on the RSOs and that this effect was cyclical. The observations also suggested that synodic effects due to RSO orbit motion could be contributing to the apparent spin periods of long spin period RSOs (greater than 1000 seconds). The most influential disturbance torque acting on these RSOs was determined to be solar radiation pressure acting on the large area solar panels. The possible cyclical variation of the RSOs' apparent spin periods suggested that the solar incidence angle on the solar panels was affected not only by the spacecraft spin but also by the Earth's orbit motion. Preliminary spin angular acceleration modelling was performed, based on varying solar radiation pressure intensity due to RSO spin and orbit motion.

I. INTRODUCTION

I.I Box-wing RSO Design

The basic *box-wing* RSO design, illustrated in Fig. 1, consists of a central cube-shaped structure (the "box") and two solar panels (the "wings"). The *wing span* (total length) can be as large as 41 metres [1].

I.II Description of Research

In this paper, an *inactive* RSO is defined as one whose attitude dynamics are influenced solely by natural forces; for example, solar radiation pressure (SRP), additional electro-magnetic forces, gravitational forces, and thermal forces.

The primary problem posed was; how to determine the attitude dynamics of an inactive box-wing GEO RSO from light curves derived from frequent (weekly) ground-based small-aperture optical photometric observations. The ancillary problems based on the primary problem included; which inactive GEO RSOs to study, how to observe the chosen RSOs, how to



Fig. 1: A Box-wing RSO

* Royal Military College of Canada, Canada, Gregg.Wade@rmc.ca.

interpret the observations, and how to analyze the preliminary findings. This paper describes how these ancillary problems were solved, what the observations suggested about each chosen RSO's spin dynamics, and the results of the preliminary analyses and modelling.

I.III Background

There have been very few published papers on the subject of long-term photometric observations of inactive box-wing GEO RSOs [2]. The most notable observations were conducted at the Russian Sayan Solar Observatory (SSO) from 1987 to 2004 [2]. SSO observed inactive Russian Raduga (Rainbow), Gorizont (Horizon), and Ekran (Eye) GEO RSOs that were similar in design to that shown in Fig. 1. Analyses of these observations conducted by Papushev et al. concluded that each GEO RSO appeared to be spinning with a varying apparent period with unique ranges and variation rates [2]. The observed spin period range was between 20 seconds and 430 seconds [2]. Papushev et al. identified tall sharp spikes and extended wide hills in the light curves that suggested specular sunlight reflections from the large area solar panels and diffuse sunlight reflections from the bus, respectively [2].

Papushev et al. suggested that the observed spin period variations were due to torques acting on the RSOs [2]. Suggested internal torques included reactivation of the RSOs' ADCS reaction wheels during favourable sunlight angles, and micro-jets caused by small holes in the hermetically sealed and pressurized

bus cabins [2]. Suggested external torques included solar radiation pressure (SRP), Lorentz (magnetic) force, and one or more collisions with debris [2].

Chu et al. identified SRP as the most influential external torque acting on the single-panel GOES-R RSO's attitude [3]. GOES-R was designed without a compensating solar sail [3]. Chu et al. estimated that without attitude control, SRP would increase GOES-R's angular momentum by an estimated 20 N·m·s in 24 hours [3].

Früh and Schildknecht studied the attitude dynamics of high area-to-mass ratio (HAMR) GEO RSOs by assuming their dimensions and reflection coefficients [4]. Comparisons between the simulated and observed light curves of these HAMR RSOs revealed that predicting the brightness (magnitude) range, spin period, and shape are particularly difficult without a priori knowledge of some of the HAMR RSOs' specifications [4].

The observed (synodic) spin period of a GEO RSO moving relative to the incoming sunlight and to the observer will appear to be larger or smaller than the RSO's actual (sidereal) spin period. Lambert et al. observed the SBS-B cylindrical RSO's synodic spin period with the Advanced Electro-Optical Sensor (AEOS) [5]. SBS-B's apparent spin period was observed to increase from under 50 seconds to nearly 200 seconds over a single night [5]. Lambert et al. hypothesized that the reasons for this increase included; a reflecting surface normal located within 10° from the spin axis orientation and a spin axis precession moving in the same direction as the motion of the reflecting surface normal motion [5].

Cylindrical RSOs' sidereal spin periods and spin axis orientations have been estimated with the Epoch Method (photometric astrometry) [6]. The available literature has not stated whether or not the method has been effective for long-term determinations or if it is also effective for observations of box-wing RSOs.

II. OBSERVATION

II.I Equipment

The hardware employed for all observations consisted of a Celestron NexStar11 GPS 0.28m (11-inch) goto equatorially-mounted Schmidt-Cassegrain telescope (SCT), a Meade 0.30m (12-inch) aperture LX-200GPS azimuth-elevation (Az-El) mounted goto SCT, a Santa Barbara Instrument Group (SBIG) ST-9XE charge coupled device (CCD) and a SBIG ST-8XE CCD.

The software employed for all observations consisted of Software Bisque's TheSkyX Professional for RSO orbit propagation and telescope control, and CCDSoft Version 5 for CCD control and automation.

II.II Preliminary RSO Selection

The RSOs had to be listed on the NORAD unclassified RSO catalogue, inactive, of box-wing design, and in a nearly circular GEO orbit. The RSOs also had to be easily detectable at night with the electro-optical equipment described in Section II.I. An RSO's minimum local elevation could not be less than 15° during any night from March 1, 2012 to March 31, 2013.

The preliminary RSOs chosen were Solidaridad-1 (NORAD #22911 [7]), Telstar-401 (#22947), Echostar-2 (#24313) and HGS-1 (formerly Asiasat-3 [8]) (#25126). In mid-2013, the Intelsat-3R (formerly PAS-3R [8]) (#23764 [7]), and Paksat-1 (formerly Anatolia-1, HGS-3 and Palapa C1 [8]) (#23779) box-wing RSOs were added.

II.III Observation Criteria and Observation Procedure

Observation Criteria

All of the RSOs were subjected to the same observation criteria. All observations were acquired from a private observatory at +44° 07' 23".8 latitude and -76° 53' 25".8 longitude. The RSO had to be at least 15° above the local horizon and have a phase angle of between 10° and 90°. The RSO could not be obstructed in any way by clouds, fog, natural structures (such as trees), or man-made structures (such as houses).

The Sun had to be 12° or more below the local horizon, and the Moon's phase had to be less than 75% when above the local horizon when observing. When above the local horizon, the Moon had to be at least 30° from the RSO's coordinates.

The RSO could not appear to be located within the Milky Way. A high density star field would have significantly increased the probability of stellar interference with an RSO's signal.

Observation Procedure

With the exception of the CCD exposure time, all of the RSOs would be subject to the same observation procedure. The telescope's sidereal tracking was switched off so that a 1-second exposure CCD image of a GEO RSO would appear as a stationary dot rather than a streak. This allowed the RSOs to remain in the CCD's field of view (FOV) for a longer time. The CCD FOV was oriented such that north (increasing declination) was at the top of the CCD image.

The observed declination of each inactive GEO RSO would increase or decrease in time because of the RSO's orbit inclination. The RSO declination's rate and direction of change was noted with additional CCD test

images. The CCD FOV was then positioned so that the RSO was observed near an image's upper or lower edge and approximately centred in the horizontal. This allowed the RSO to drift along the FOV's vertical axis as CCD images were obtained. The time for an RSO to drift through the FOV varied from 3 minutes to 30 minutes.

The default CCD exposure time per image was 1 second with a CCD chip temperature set between -30°C and -15°C. This exposure time maximized the sampling frequency and provided a satisfactory RSO signal. If required, the CCD exposure time was decreased or increased by 0.5 seconds. All images were automatically dark current subtracted in real time. The CCD duty cycle was determined to be 3.3 seconds for a 1-second exposure time.

Once the RSO had reached the opposite edge of the FOV, the telescope was manually slewed in declination to place the RSO near the starting point in the CCD FOV. The RSO was allowed to drift through the FOV again. This procedure was repeated until the desired observation time had passed, normally between 45 minutes and two hours. A *block* was defined as a group of images during which the RSO drifted through the FOV once.

When weather and accessibility permitted, all RSOs would be observed at a minimum of twice per week, normally separated by at least two days.

II.IV Image Analysis Software

The raw data typically consisted of up to 10,000 CCD images per night. The photometric data points had to be extracted from each image in a timely manner. For this reason, image analysis software was developed in MATLAB. The software extracts the Network Time Protocol (NTP) time tag and determines the RSO's photometric brightness from each image.

The software rejects any signal distribution in which the absolute difference between the x-axis size and the y-axis size is greater than 3 pixels, so that most stellar and wind interference with the RSO signal is discounted.

The combination of the time tags and the photometric data created the light curves. Example light curves for each RSO are shown in Section II.V.

II.V Light Curves

Example light curves are shown in Fig. 2 (Intelsat-3R), Fig. 3 (Telstar-401), Fig. 4 (Paksat-1), Fig. 5 (Echostar-2), Fig. 6 (Solidaridad-1), and Fig. 7 (HGS-1). Each RSO light curve represents one of many obtained for each RSO.

Despite the similar box-wing RSO designs, the light curve characteristics of each RSO typically appeared

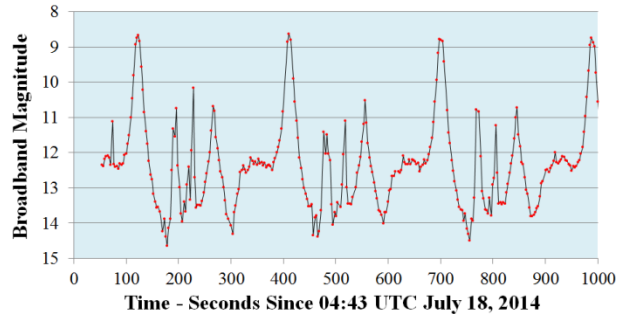


Fig. 2: A Single Light Curve of Intelsat-3R

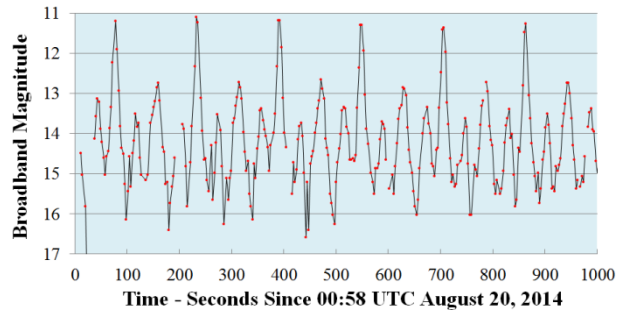


Fig. 3: A Single Light Curve of Telstar-401

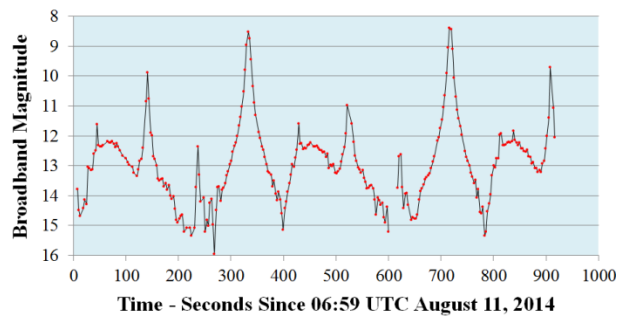


Fig. 4: A Single Light Curve of Paksat-1

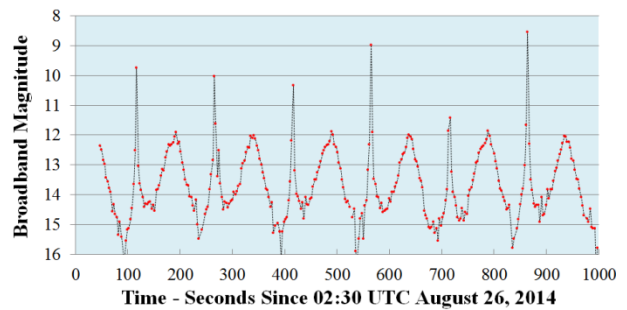


Fig. 5: A Single Light Curve of Echostar-2

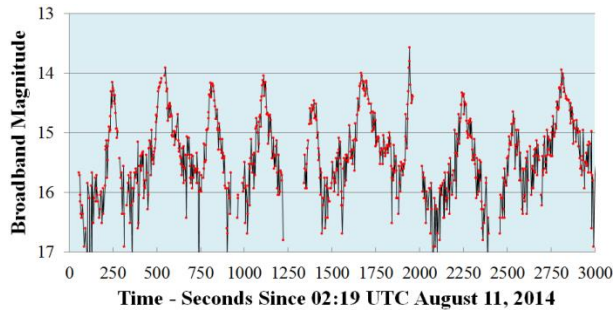


Fig. 6: A Single Light Curve of Solidaridad-1

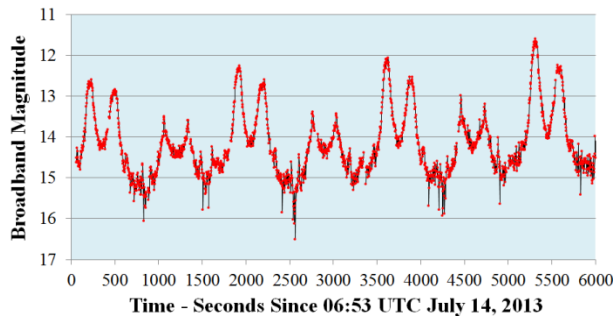


Fig. 7: A Single Light Curve of HGS-1

different from the others. However, some light curves exhibited alternating “tall spike” and “wide hill” distributions which might have indicated which part of the RSO the sunlight was being reflected from. In some cases, the tall spike was observed to be superimposed onto a wide hill.

Although they might have appeared unchanging over a few apparent periods, the light curve characteristics were typically observed to change over a few hours to several days. For instance, the tall spike maximum was observed to shrink or grow over a single night. The wide hill also appeared to change but not as dramatically as the tall spike. In rarer instances, the tall spike’s maximum was seen to increase by several magnitudes in one night, which might have indicated that the sunlight was being reflected nearly directly to the observer. This might be one of a number of indicators of the instantaneous RSO attitude. These bright flares were observed for many of the RSOs at some time during their observations.

II.VI Spin Period Determination

Manual Spin Period Determination

The light curves demonstrated, at face value, that the sampling frequency was larger than the Nyquist frequency. However, the imaging cadences required to resolve different characteristics (such as a tall spike and

a wide hill) were not the same. The tall spike was better localized in time and could be considered closest to a delta function. Therefore, maximum RSO signal in a tall spike was preferred over other characteristics when manually determining the spin period.

In most cases, the light curves suggested that the apparent RSO spin period could be determined by identifying similar prominent light curve characteristics, and by measuring the time elapsed between two adjacent similar characteristics, such as maxima of tall spikes. An inspection of Fig. 3 led to the detection of four unique characteristics, illustrated in Fig. 8, which were used to determine Paksat-1’s apparent spin period.

Characteristic #1 appears three times in Fig. 8 and is most likely a specular reflection. The time between the first and second occurrence of this characteristic was measured to be 384 ± 4 seconds. Similarly, the time between the second and third occurrences of characteristic #1 was measured to be 386 ± 4 seconds. The time between adjacent occurrences of characteristics #2, #3 and #4 were similar, with the time between occurrences of characteristic #4 indicated in Fig. 8.

The uncertainty was reduced by determining the elapsed time between the extreme similar characteristics and dividing the result by the number of apparent periods between them. For example, the elapsed time between the first and third occurrences of characteristic #1 in Fig. 8 was measured to be 770 ± 4 seconds. Dividing this result by 2 apparent periods yielded 385 ± 2 seconds. Figure 3 and Fig. 8 show a subset of the observations of Paksat-1 obtained on a single night. A total of 10 apparent spin periods were actually observed. The first and last occurrences of characteristic #2 in the complete light curve yielded the result of 384.4 ± 0.4 seconds. This method was used to determine the apparent spin periods of Intelsat-3R, Telstar-401, Paksat-1, and Echostar-2. In these cases, the variations of the apparent spin periods within a light curve, when measured using adjacent similar characteristics, appeared to be negligible. However, the apparent spin periods of Solidaridad-1, and HGS-1 appeared to deviate by as much as 20 seconds (much larger than

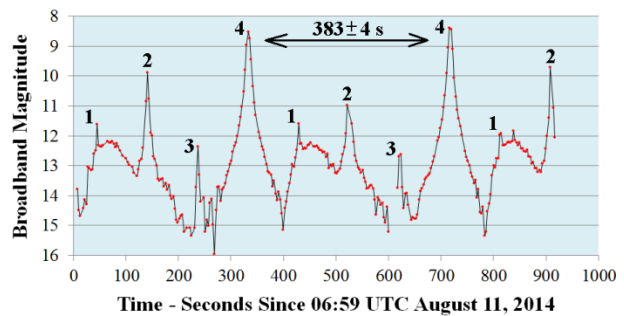


Fig. 8: Four Light Curve Characteristics of Paksat-1

the 3.3s uncertainty) between adjacent pairs. This puzzling behaviour indicated that using extremes could not be used to determine the overall apparent spin period in these cases, unless an average spin period was required.

Solidaridad 1's, and HGS-1's spin period uncertainties were determined by measuring the overall minimum and the maximum observed spin periods and dividing this difference by 2.

Lomb-Scargle Spin Period Determination

A Lomb-Scargle [9] analysis of the light curves was used for comparison with the manual method. The Lomb-Scargle method was not used for Solidaridad-1 and HGS-1 because of their apparently varying spin periods over a single light curve. In this paper, the complete Paksat-1 light curve, of which Fig. 3 and Fig. 8 are subsets, was used as the example of a typical Lomb-Scargle analysis.

The Lomb-Scargle analysis first produced a periodogram that indicated the most likely oscillation frequencies, as shown in Fig. 9. The most likely frequency shown is 0.0052065 Hz, which corresponds to an apparent spin period of 192.07 seconds.

A significant problem encountered when using the Lomb-Scargle analysis was that it appeared to determine oscillations without considering the similar light curve characteristics. However, multiples of the determined periods could be tested using folded phase plots. The phase plot corresponding to the correct apparent spin period of Paksat-1 is shown in Fig. 10. This phase plot corresponds to a period of 384.6 seconds, which verifies the spin period determined by the manual analysis within the 0.4-second uncertainty.

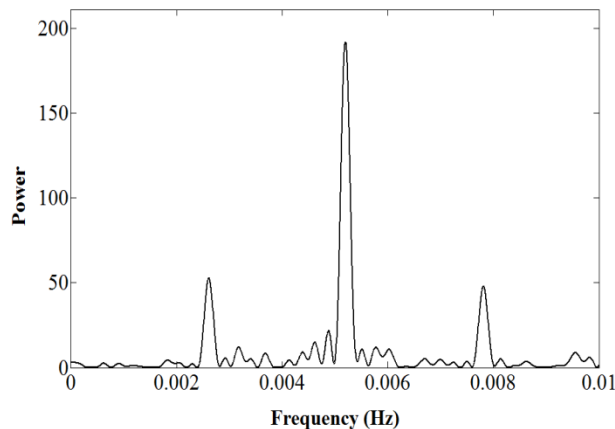


Fig. 9: A Lomb-Scargle Periodogram of Paksat-1 showing Frequencies between 0 and 0.01 Hz.

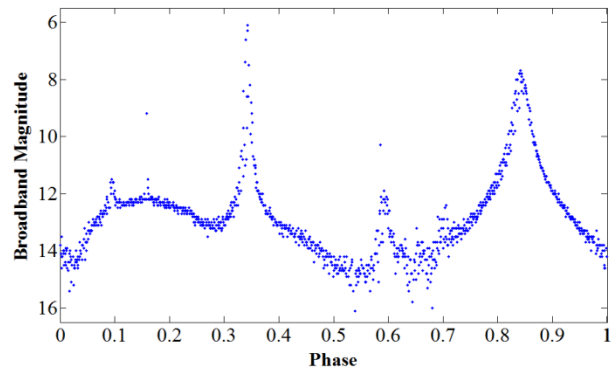


Fig. 10: Phase Plot of Paksat-1 based on a Multiple of the Period Determined from Fig. 9.

II.VII Eclipses

Several weeks before and after the Vernal Equinox and the Autumnal Equinox, the RSOs were eclipsed by the Earth for a maximum of 70 consecutive minutes each day.

In order to determine if eclipses affected RSO spin periods, several light curves were obtained of Telstar-401, Echostar-2, Solidaridad-1, and HGS-1 immediately before and after maximum duration eclipses. The differences between the pre-eclipse and post-eclipse spin periods did not deviate by more than the observational uncertainties. Therefore, none of these observations suggested that eclipses affected the RSOs' spin periods.

II.VIII Apparent Spin Period Variations

The RSO spin period was determined from each light curve. The resulting apparent spin period plots are shown in Fig. 11 (Intelsat-3R), Fig. 12 (Telstar-401), Fig. 13 (Paksat-1), Fig. 14 (Echostar-2), Fig. 15 (Solidaridad-1), and Fig. 16 (HGS-1). An error bar is shown if it is larger than its corresponding data point size.

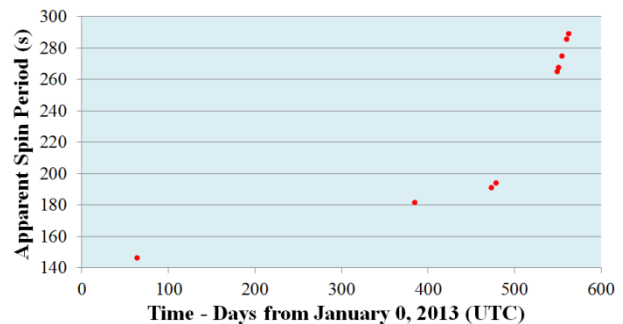


Fig. 11: Spin Period Variation of Intelsat-3R

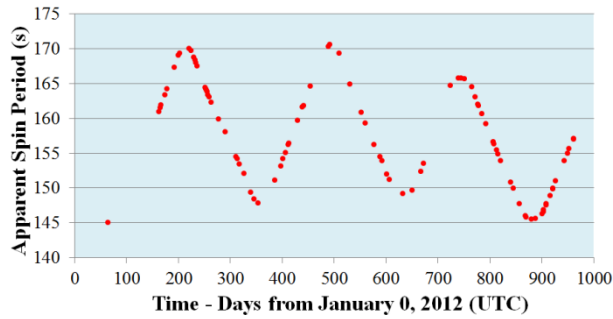


Fig. 12: Spin Period Variation of Telstar-401

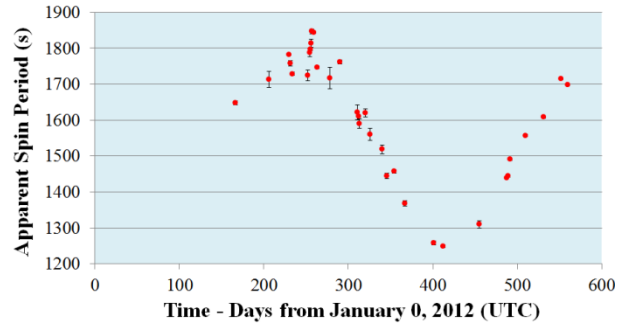


Fig. 16: Spin Period Variation of HGS-1

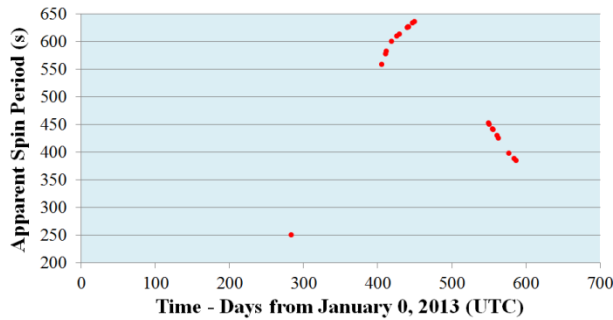


Fig. 13: Spin Period Variation of Paksat-1

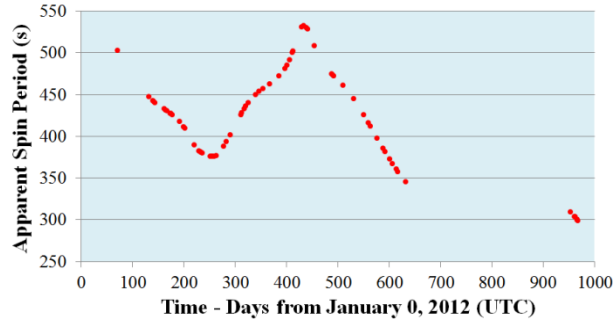


Fig. 14: Spin Period Variation of Echostar-2

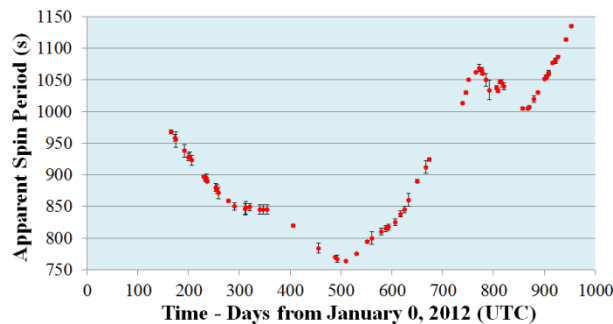


Fig. 15: Spin Period Variation of Solidaridad-1

Each RSO was observed to have a varying apparent spin period. The spin period variation characteristics appeared different from one another, especially in shape and in amplitude. Several of the spin period variations, most notably those for Telstar-401 (Fig. 12), Paksat-1 (Fig. 13), Echostar-2 (Fig. 14), Solidaridad-1 (Fig. 15), and HGS-1 (Fig. 16) appeared to be varying in a cyclical manner.

Spin period variation indicates an angular velocity variation, i.e. angular acceleration. Therefore, these variations strongly suggest that one or more torques are acting in some manner on each RSO. This is discussed in more detail in Section III.

The spin period variations of Echostar-2 (Fig. 14) and Solidaridad-1 (Fig. 15) show a very curious feature, resembling a point of inflection. At areas along the curve, the absolute spin period slope appears to decrease for some time before resuming its original slope. These features resemble a “bump” along the curves. For Echostar-2 (Fig. 14), two bumps occur, one between days 100 and 200 and the other between days 450 and 500. For Solidaridad-1 (Fig. 15), two bumps occur, one between days 300 and 400 and possibly another between days 800 and 900. The second Solidaridad-1 bump does not resemble the others and the spin period appears to oscillate with dampening amplitude before the spin period slope resumes its increase.

Telstar-401’s spin period variation (Fig. 12) also shows bumps but they are more difficult to detect. The most recent Paksat-1 plot (Fig. 13) also suggests a bump feature around day 600, but additional observations are required to confirm this.

If the spin period variations are periodic, then the periods would be different from each other. The apparent variation period of Telstar-401 appears smaller than the others and also appears to vary over time, so far ranging from 250 days to 290 days.

The variation amplitude (A) appears to increase with the average spin period (\bar{T}), as illustrated in Fig. 17. Figure 17’s green data points indicate well-known variation amplitudes based on several apparent periods. The orange data points indicate that a single minimum-maximum pair has been identified and more data are

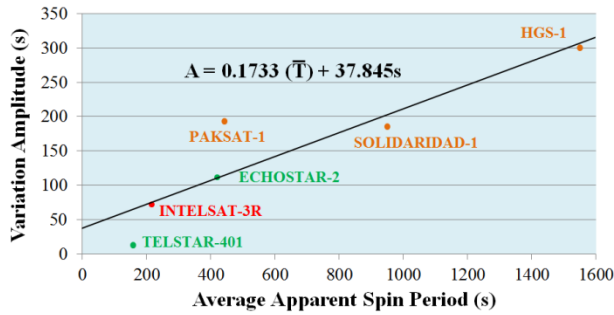


Fig. 17: Spin Period Variation Amplitude vs. Average Apparent Spin Period.

required to confirm their values. The red data point indicates that a minimum, maximum or both have not yet been identified and that more data are required. Assuming that the possible relationship is linear, the least-squares linear equation is also displayed in Fig. 17.

II.IX Apparent Angular Acceleration

The apparent spin angular acceleration (α_{spin}) was calculated from the adjacent spin periods (T_1 and T_2) and the elapsed time between them (Δt) with Eq. 1.

$$\alpha_{spin} = \frac{2\pi}{\Delta t} \left[\frac{1}{T_2} - \frac{1}{T_1} \right] \quad (1)$$

The plots of apparent spin angular acceleration over time are shown in Fig. 18 (Intelsat-3R), Fig. 19 (Telstar-401), Fig. 20 (Paksat-1), Fig. 21 (Echostar-2), Fig. 22 (Solidaridad-1), and Fig. 23 (HGS-1).

The bump feature seen in Telstar-401's (Fig. 12) and Echostar-2's (Fig. 14) spin period variations can be seen in their corresponding angular acceleration plots as local maxima and minima in between the zero crossings. The bumps are not clearly visible in Solidaridad-1's angular acceleration plot (Fig. 22), possibly because its spin period uncertainties are much larger than those measured for Telstar-401 and Echostar-2.

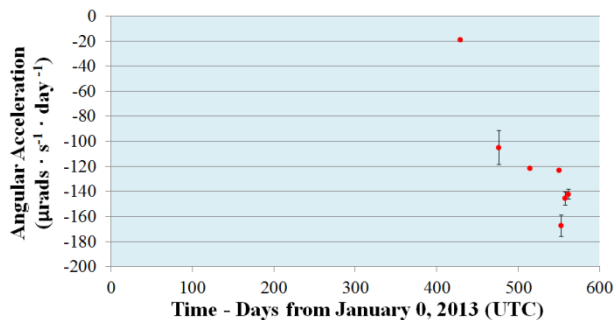


Fig. 18: Angular Acceleration of Intelsat-3R

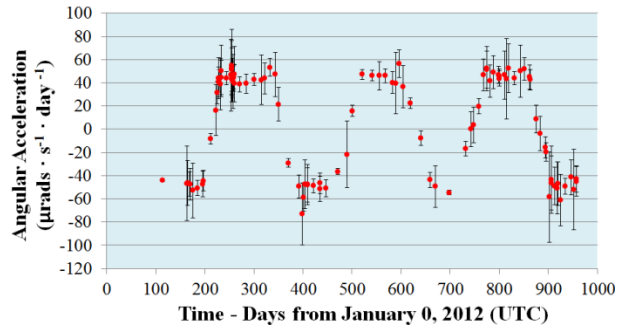


Fig. 19: Angular Acceleration of Telstar-401

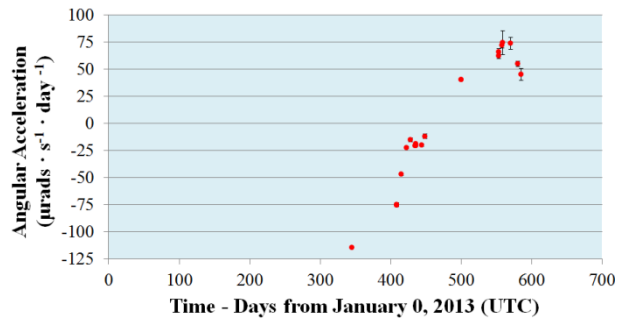


Fig. 20: Angular Acceleration of Paksat-1

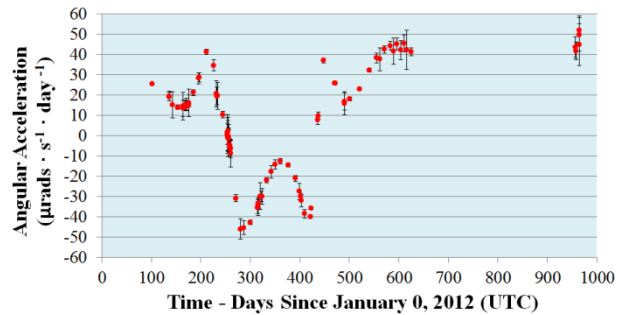


Fig. 21: Angular Acceleration of Echostar-2

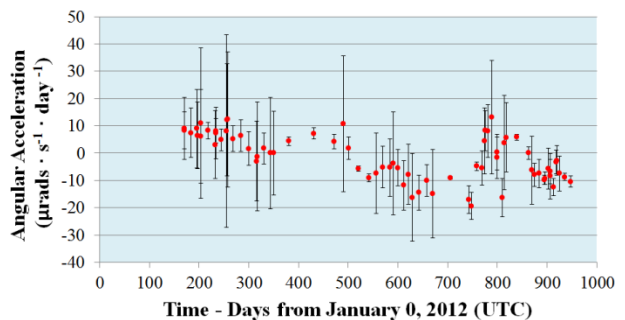


Fig. 22: Angular Acceleration of Solidaridad-1

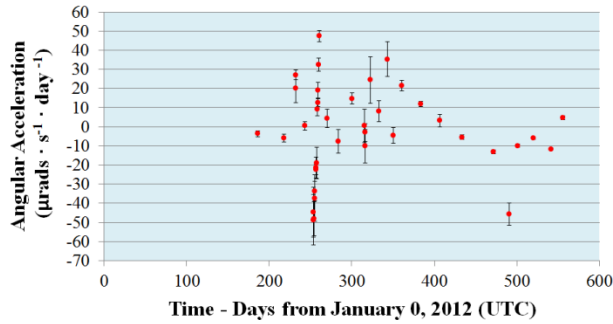


Fig. 23: Angular Acceleration of HGS-1

The apparent angular accelerations of Telstar-401, Paksat-1, Echostar-2, and HGS-1 appear to be varying within equal-magnitude boundaries. For example, Telstar-401’s angular acceleration appears to vary between -60 and +60 $\mu\text{rad} \cdot \text{s}^{-1} \cdot \text{d}^{-1}$. Echostar-2’s angular acceleration appears to vary between -50 and +50 $\mu\text{rad} \cdot \text{s}^{-1} \cdot \text{d}^{-1}$ with the bumps having local minima and maxima at approximately -10 and +10 $\mu\text{rad} \cdot \text{s}^{-1} \cdot \text{d}^{-1}$, respectively.

Intelsat-3R’s apparent angular acceleration variation appears much faster than those of Telstar-401, Echostar-2 and Solidaridad-1. The sudden apparent reversal of HGS-1’s angular acceleration (Fig. 23) from -50 to +50 $\mu\text{rad} \cdot \text{s}^{-1} \cdot \text{d}^{-1}$ near day 250 is also an interesting observation.

The largest apparent angular acceleration magnitudes (α_{max}), determined from Fig. 18 to Fig. 23, are shown in Table 1. These values were compared to all maximum calculated hypothetical torques to determine if they could accelerate each RSO’s spin at these observed rates.

RSO	α_{max} ($\mu\text{rad} \cdot \text{s}^{-1} \cdot \text{d}^{-1}$)
Intelsat-3R	167 ± 9
Telstar-401	73 ± 27
Paksat-1	114.3 ± 0.2
Echostar-2	46 ± 5
Solidaridad-1	19 ± 5
HGS-1	49 ± 13

Table 1: Maximum Observed Angular Acceleration Magnitudes

III. ANALYSIS

At the beginning of this research, a number of hypotheses were considered to explain the observed RSOs’ angular accelerations, with the understanding that one, several or all of them could be correct.

III.I Moment of Inertia

Any torque’s ability to apply an angular acceleration depends on the rigid body’s moment of inertia (MOI) (also called rotational inertia). The MOI depends on the body’s mass, dimensions, and its principal spin axis orientation.

With the exception of HGS-1, each RSO was assumed to be comprised of a single uniform density cube with two flat plates attached to opposite sides of the cube, as illustrated in Fig. 24 (top). All other RSO components were assumed to have negligible masses. Only one of the two HGS-1 solar panels successfully deployed after launch [8]. Therefore, HGS-1 was assumed to be comprised of a single uniform density cube with a deployed flat plate attached to one side of the cube and a smaller flat plate with the same mass as the first plate lying flat against the opposite side of the cube, as illustrated in Fig. 24 (bottom). In both cases, the principal spin axis was assumed to be running through the center of the cube and perpendicular to the cube sides not coincident with the plate attachments, as illustrated in Fig. 24.

The MOIs of the RSO configurations shown in Fig. 24 (top and bottom) were determined with Eq. 2 and Eq. 3, respectively. In Eq. 2 and Eq. 3, I is the MOI, m_{box} is the mass of the cube, and m_{panel} is the mass of a single solar panel.

$$I = \frac{1}{6} \{ m_{\text{box}} a^2 + m_{\text{panel}} [4l_{\text{panel}}^2 + 3l_{\text{tot}}(l_{\text{tot}} - 2l_{\text{panel}})] \} \quad (2)$$

$$I = \frac{1}{6} m_{\text{box}} a^2 + m_{\text{panel}} \left[l_{\text{tot}}^2 + \frac{65}{192} l_{\text{panel}}^2 + (a + l_{\text{panel}}) \left(\frac{1}{2} a - l_{\text{tot}} \right) \right] \quad (3)$$

Determining the RSOs’ dimensions and masses was the most difficult effort of this research so far because of the lack of peer-reviewed references containing RSO design specifications. RSO dimensions were determined by interpolation from web-published wing spans and

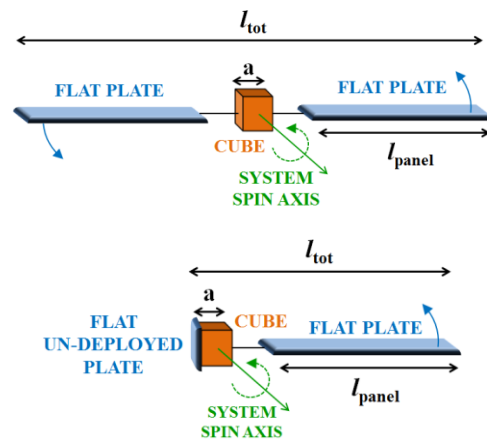


Fig. 24: Conceptual Illustrations of Two-panel RSOs (top) and the HGS-1 Single-panel RSO (bottom)

from artist conceptions of the RSOs or their designs. RSO mass was determined from the web-published on-orbit mass, the dry mass and the estimated remaining manoeuvring fuel mass. Uncertainties for each dimension and mass were estimated. The MOI estimated for each RSO is shown in Table 2.

RSO	DESIGN [8]	I (kg · m ²)
Intelsat-3R	HS-601HP	10500 ± 830
Telstar-401	AS-7000	10100 ± 1000
Paksat-1	HS-601	5240 ± 690
Echostar-2	AS-7000	9510 ± 930
Solidaridad-1	HS-601	5450 ± 740
HGS-1	HS-601HP	6320 ± 520 [†]

Table 2: Estimated MOIs

III.II External Torques

External torques are constantly being applied to each RSO. These include solar radiation pressure (SRP), solar wind pressure, Lorentz (magnetic) forces, gravitational forces (from the Earth, Sun and Moon), thermal forces, and interactions with artefacts, such as meteoroids or man-made orbiting debris. To be considered a significant contributor to RSO spin angular acceleration, an external torque needed to be strong enough to systematically apply an angular acceleration to each RSO that was equal to or greater than the corresponding maximum observed angular accelerations stated in Table 1. The characteristics of the candidate external torque also had to be present, at least in part, in the observed characteristics of the spin period variations and angular accelerations.

If thermal torques were the main cause of the angular accelerations, large variations during each eclipse season should have been observed because of fast cooling (during eclipse) and fast heating (after eclipse). Thermal torque was discounted early in the research because significant variations were not observed immediately after eclipses, and Telstar-401's and Echostar-2's bumps were not observed to be coincident with their eclipse seasons.

The Earth's magnetosphere grows and shrinks (sometimes exposing the GEO RSOs) according to the Sun's somewhat unpredictable activity. If solar wind was the primary external torque, then the observed RSOs' angular accelerations should have correlated with the solar proton density, especially during coronal mass ejections (CMEs) that were directed toward the Earth. No correlations of this type were found; therefore solar wind torque was discounted early in the research.

A gravity-gradient stabilized GEO RSO can oscillate during its sidereal day orbit period [10]. However, no

evidence was found suggesting that the spin period variation oscillated in 24-hour periods.

Gravitational effects from the Moon were discounted early in this research because none of the spin period variation features appeared to correlate with the Moon's 27.3-day orbit period.

If an inactive RSO collides with an artefact, the change in its spin axis should be sudden and not systematic. Interaction with artefacts was considered in this research because of the curious observations of Solidaridad-1 after day 800 (Fig. 15). Solidaridad-1's spin period was expected to slowly and steadily decrease, encounter a bump, and then reach minimum again. Instead, the curve sharply turned, began oscillating and then increased once again. This might be evidence that Solidaridad-1 had collided with a small artefact and had its spin axis orientation abruptly changed.

The remaining contenders (SRP and magnetic forces) were compared by estimating their maximum possible torque on each RSO. Magnetic torque was assumed to be caused solely by the RSO's interaction with the Earth's magnetic field. SRP torque was assumed to be caused solely by broadband sunlight.

The maximum angular acceleration due to magnetic torque was estimated with Eq. 4. In Eq. 4, α_{mag} is the angular acceleration due to magnetic torque, D is the total residual magnetic dipole moment (assumed to be 1 A·m² for each RSO), M_{Earth} is the magnetic moment of the Earth (7.96×10^{15} T·m³ [10]), and R is the radial distance from the center of the Earth (4.2253×10^7 m). The results are shown in Table 3.

$$\alpha_{\text{mag}} = \frac{DM_{\text{Earth}}}{IR^3} \quad [10] \quad (4)$$

The maximum angular acceleration due to SRP torque was estimated by assuming that the incident sunlight was orthogonal to one of the two solar panels at some time during the RSO spin and that the second solar panel was oriented orthogonally to the first solar panel. In this scenario, the second solar panel would not be illuminated at any time during the RSO's spin, ensuring that the second panel would not negate the angular acceleration from the first panel. One side of the first panel was assumed to have a reflectivity (q_1) of 0.6, and the opposite side was assumed to have a reflectivity (q_2) of 0. The maximum SRP angular acceleration magnitude was calculated over a single RSO spin using Eq. 5. In Eq. 5, α_{SRP} is the angular acceleration magnitude due to SRP, P_{rad} is the solar radiation pressure at a distance of 1 astronomical unit (A.U.) from the Sun (4.537×10^{-6} Pa [10]) and A_{panel} is the area of the solar panel. The results are shown in Table 3.

$$\alpha_{\text{SRP}} = \frac{P_{\text{rad}}A_{\text{panel}}(l_{\text{tot}} - l_{\text{panel}})|q_2 - q_1|}{I\pi} \quad [10] \quad (5)$$

[†] Based on a single deployed solar panel

RSO	α_{mag} ($\mu\text{rad} \cdot \text{s}^{-1} \cdot \text{d}^{-1}$)	α_{SRP} ($\mu\text{rad} \cdot \text{s}^{-1} \cdot \text{d}^{-1}$)
Intelsat-3R	0.87 ± 0.07	2600 ± 400
Telstar-401	0.90 ± 0.09	3000 ± 500
Paksat-1	1.7 ± 0.2	3000 ± 700
Echostar-2	0.96 ± 0.09	3200 ± 500
Solidaridad-1	1.7 ± 0.2	2900 ± 700
HGS-1	1.44 ± 0.11	4300 ± 600

Table 3: Maximum Angular Acceleration Magnitudes due to Magnetic and SRP Torques

The results in Table 3 were compared to those in Table 1. It was concluded that SRP was the most likely external torque acting on the RSOs and that the magnetic torques were not sufficient to accelerate the RSOs at their maximum values.

A comparison of Table 1 with Table 3 suggested that the absolute difference between the solar panel's q_1 and q_2 values do not have to be as high as 0.6 in order for SRP to cause the observed angular acceleration magnitudes. The same aforementioned solar panel scenario was used to determine the minimum absolute difference between q_2 and q_1 by rearranging Eq. 5 and using the maximum observed angular accelerations (α_{max}) from Table 1 for α_{SRP} values of each RSO. The resulting absolute reflectivity difference was on the order of 10^{-4} . This demonstrated that the effect of the SRP torque was significant even for very small reflectivity differences.

III.III Internal Torques

Attitude Control Reactivation

The onboard power systems of one, several or all of the RSOs might have been semi-operational during the observations because the solar panels were still operational when in sunlight. Furthermore, each ADCS might have been receiving power during favourable sunlight illuminations on the solar panels [2]. In this case, an ADCS might still attempt to control an inactive RSO's attitude.

The status of each ADCS has likely been unknown since the RSO's end of life (EOL). If the ADCS was to suddenly become active and attempt to stabilize an RSO's attitude, then the observed angular acceleration would likely change within minutes. If an ADCS was reactivated, it would not likely remain active for very long because the RSO spin would only allow a brief time of adequate solar illumination on the panels.

To date, there has been no observed evidence of large spin period changes over a small time frame. The puzzling spin period change of Solidaridad-1 near day 800 is unlikely the result of a sustained ADCS reactivation because no unusual changes in its light

curve were observed between day 792 and day 806 since January 0, 2012.

Fuel Slosh

Several of the RSOs suffered catastrophic failures a number of years before their designed EOLs [8]. As a result, onboard manoeuvring fuel was not fully depleted. If unspent fuel can slosh within the fuel tanks, there is a possibility that the resulting internal torque could change the RSO's attitude. However, the fuel tanks are located within the box portion; near the RSO's center of mass. Therefore, the internal torque might be very small, especially if the mass of the remaining fuel is small. Fuel slosh can only occur if a sudden change in orbital or attitude acceleration occurs.

The bumps in the angular accelerations did not occur suddenly, but over several weeks. Telstar 401's and Echostar-2's local maxima and minima during the bumps were observed to have had similar magnitudes. A fuel slosh would likely not produce these smoothly varying observations. However, Solidaridad-1's curious spin period variation oscillation between days 792 and 868 could suggest slow fuel slosh after a sudden change in angular acceleration.

Micro-jets

Assuming that the RSOs were pressurized when active, a small hole would have resulted in a micro-jet torque [2]. However, over time the angular acceleration should have constantly decreased as the internal bus pressure equalized with the very low external pressure. Telstar-401 has been inactive since early 1997, making it unlikely that a micro-jet could have sustained its apparent angular acceleration for nearly two decades. Telstar-401's maximum and minimum angular acceleration magnitudes appeared steady over 2.5 years. Therefore, the micro-jet hypothesis is not supported by the observations.

III.IV Synodic Effects

A synodic effect is the result of relative motion that causes the appearance of a modification of an RSO's kinematic state. For example, the apparent stationary appearance of a GEO RSO as observed from the Earth's surface is a synodic effect caused by the nearly equal angular velocities of the Earth's rotation and the RSO's orbit motion.

Phase Angle Bisector

The *phase angle bisector* (PAB) is defined as the line that bisects the RSO phase angle into two equal half-angles corresponding to the sunlight incidence

angle on a reflecting surface [6], as illustrated in Fig. 25. Figure 25 shows the phase angle (ρ), the PAB (β) and the normal unit vector to the reflecting surface (\hat{n}).

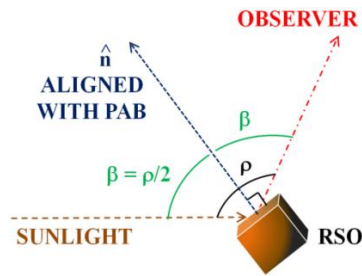


Fig. 25: The Phase Angle Bisector Aligned with RSO Surface Normal

Synodic Spin Period

The synodic spin period is the apparent time elapsed between an observed reflection from an RSO and the next reflection from the same surface to the same observer. If there is no relative motion between the RSO, the observer and the incident sunlight, then the synodic spin period is the same as the sidereal spin period. Since the RSOs studied were in motion with respect to the incoming sunlight during the observations, all observed apparent spin periods shown in Fig. 11 to Fig. 16 were synodic spin periods.

The magnitude of the synodic effect on a GEO RSO spin period (as viewed from the Earth’s surface) will depend primarily upon on two criteria: the true (sidereal) RSO spin period and the orientation of the RSO’s spin axis with respect to the RSO’s phase angle bisector (PAB). A GEO RSO with a long sidereal spin period and a small angle between the spin axis and PAB will be more susceptible to synodic effects than a GEO RSO with a short spin period and a larger angle between the spin axis and the PAB.

An example of the difference between the synodic period and the sidereal period of a spinning GEO RSO is illustrated in Fig. 26. In this scenario, the reflecting surface normal (\hat{n}) is at an angle ψ with respect to a spin axis orthogonal to the RSO’s orbit plane. An observer at point O_1 first views a specular reflection from the RSO at point P_1 . One sidereal spin period later, the RSO’s surface normal is no longer aligned with the PAB because the orbit motion has changed the perspective with respect to the incident sunlight. The RSO needs to spin more than one sidereal spin period in order for the observer at O_2 to see another reflection from the RSO. When the RSO has reached point P_2 , it has spun with the synodic spin period and its surface normal has realigned with the PAB. The Earth-bound observer will have observed the synodic spin period.

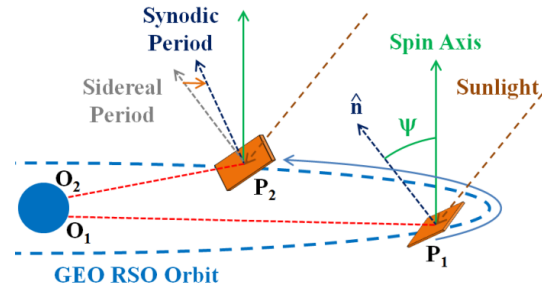


Fig. 26: The Observed Synodic Spin Period of a Spinning GEO RSO

The synodic spin period can be smaller or larger than the sidereal spin period depending on the orientation of the spin axis, which can range from $-\pi/2$ to $+\pi/2$ radians from the orbit plane. The general solution to the synodic problem is more complex; however the scenario shown in Fig. 26 conveys the basic concept.

Assuming the RSO spin axis orientation shown in Fig. 26, the difference (ΔT) between the synodic spin period (T_{syn}) and the sidereal spin period was determined using Eq. 6, where T_{GEO} is the GEO RSO orbit period (one sidereal day). The resultant plot of ΔT vs. T_{syn} for different values of ψ is shown in Fig. 27.

$$\Delta T = T_{syn} \left\{ 1 - \left\{ 1 + \frac{1}{2\pi} \cos^{-1} \left[1 + \frac{\cos \left[\pi \left(\frac{T_{syn}}{T_{GEO}} \right) \right] - 1}{\sin^2 \psi} \right] \right\}^{-1} \right\} \quad (6)$$

Fig. 27 shows that ΔT increases as a GEO RSO’s synodic spin period increases and as the angle ψ decreases. Therefore, longer spin period RSOs, such as HGS-1, will be more susceptible to synodic effects than the shorter spin period RSOs, such as Telstar-401 and Intelsat-3R.

According to Fig. 27, if the RSOs’ spin axes orientations were as shown in Fig. 26, then the synodic spin periods of Telstar-401, Intelsat-3R, Echostar-2 and Paksat-1 could have been similar to their sidereal spin

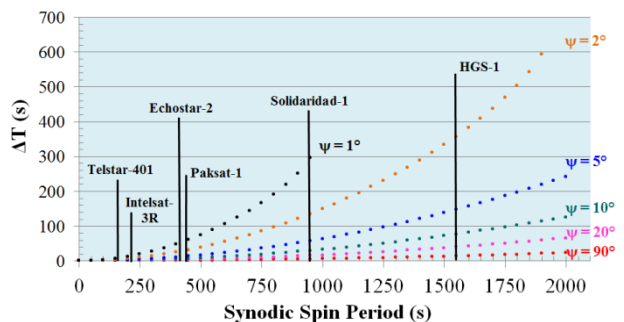


Fig. 27: GEO RSO Synodic-Sidereal Spin Period Difference (ΔT) vs. the Synodic (Observed) Spin Period (T_{syn}) based on Fig. 26 and Eq. 6.

periods as long as their ψ angles were greater than 20° . The RSOs with the longest apparent spin periods (Solidaridad-1, and HGS-1) should have had larger differences between their synodic and sidereal spin periods. This might explain why the spin periods of Solidaridad-1, and HGS-1 appeared to change with each measurement.

Telstar-401's and Instelsat-3R's measured spin period variations and angular accelerations were assumed to be the closest to sidereal because these RSOs were likely the least susceptible to synodic effects, according to Fig. 27. The apparent bumps measured for Telstar-401 (Fig. 12) appeared smaller than those measured for Echostar-2 (Fig. 14), which in turn appeared smaller than those for Solidaridad-1 (Fig. 15). This phenomenon might suggest that the bumps had been caused by synodic effects. However, the ψ angle is another free parameter that cannot be ignored. Unfortunately the true value of the ψ angle was unknown for all determined spin periods; therefore this phenomenon could be purely coincidental.

A problem with this hypothesis is that most RSOs are comprised of many facets whose surface normals can point in different directions and at different ψ angles. Therefore, sunlight reflections from these varied surfaces should result in unique synodic spin periods. Preliminary analyses of different light curve characteristics of long synodic spin period RSO's have not resulted in a dependence on the chosen light curve characteristic.

III.V Preliminary Modelling of RSO Attitude Dynamics

Assuming that a RSO's spin axis is fixed in inertial space, the angle between the RSO spin axis vector and the sunlight vector will not change substantially over 24 hours. However, as the Earth orbits the Sun, this angle will change with a 365.2422 day period. As a result, the sunlight incidence on the spinning RSO's solar panels will also vary, as illustrated in Fig. 28. This effect could affect the observed light curve over a time span of days or weeks and change the SRP torque on the solar panels, subsequently changing the net angular acceleration magnitude.

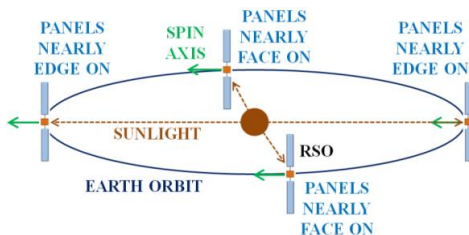


Fig. 28: Varying Incident Sunlight on RSO Solar Panels over Earth's Orbit Period.

Effects of Canted Solar Panels

The very small reflectivity difference between a solar panel's sides determined in Section III.II prompted an investigation into the relative orientation of both RSO solar panels. It was highly unlikely that both RSO solar panels were oriented exactly the same in inertial space. Therefore, it was logical to assume that there was some canting angle (ϕ) between the solar panels, as illustrated in Fig. 29. Figure 30 shows the same panel orientations viewed from along the longest axis of the RSO and orthogonal to the sunlight vector. Figure 31 illustrates the variation of the solar incidence angle on the two solar panels shown in Fig. 29 and Fig. 30 over one Earth orbit. In Fig. 31, ω qualitatively illustrates the RSO's instantaneous spin angular velocity, α qualitatively illustrates the RSO's spin angular acceleration due to SRP, and t_i represents the time.

Figure 29, Fig. 30, and the RSO depicted at time t_0 in Fig. 31 represent the same sunlight incidence angles on the panels. At time t_0 , both panels are shown to have the same solar incidence angles. Assuming that both panels have the same reflectivity, the net angular acceleration should be 0 because the SRP torques are equal and opposite. At time t_1 in Fig. 31, the sunlight incidence angle of the blue (bottom) panel has become smaller than the sunlight incidence angle of the red (top) panel. Therefore, the SRP torque of the blue panel will be greater than that of the red panel. The result will be a net angular acceleration that will assist the spin's

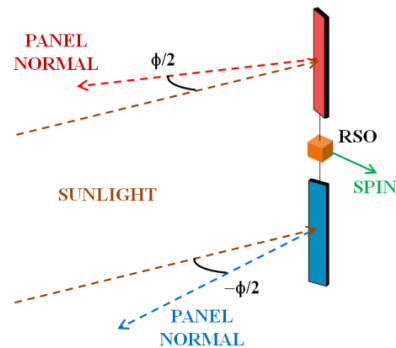


Fig. 29: Canted Solar Panels. Angles exaggerated for illustrative purposes.

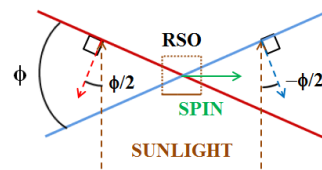


Fig. 30: Solar Panel Orientation of Fig. 29 viewed along the RSO's Long Axis. Angles exaggerated for illustrative purposes.

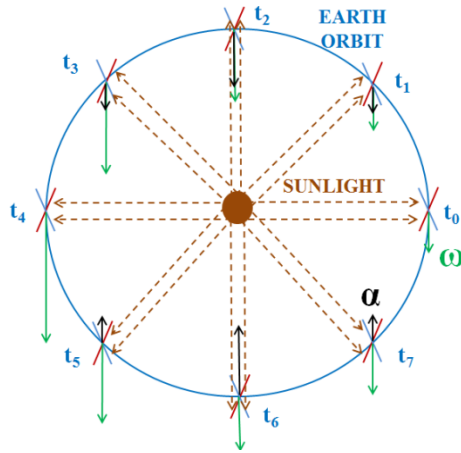


Fig. 31: Solar Incident Angle on RSO Solar Panels over an Earth Orbit. Angles and vectors exaggerated for illustrative purposes.

angular velocity vector, decreasing the spin period. At time t_2 , the sunlight incidence angles are equal, but both of the panels are assisting the spin, thereby resulting in a larger spin angular acceleration in the direction of the angular velocity vector, further decreasing the spin period. The bumps seemed to occur at or near this area. At time t_3 , the sunlight incidence angle on the red panel is smaller than the sunlight incidence angle on the blue panel, thus assisting the angular velocity but with a smaller net angular acceleration than at time t_2 . At time t_4 , both of the sunlight incidence angles are the same and the net angular acceleration is 0.

At time t_5 in Fig. 31, the net angular acceleration is opposing the spin angular velocity, thus the spin period reaches a minimum at time t_4 and begins to increase after that. The maximum opposing net angular acceleration occurs at time t_6 when both sides of the panel are spinning against the SRP. At time t_7 the opposing net angular acceleration shrinks and the spin period increases with a smaller rate than that at time t_6 . The cycle begins again after one Earth orbit.

Figure 31 suggests that the spin period variation would be cyclical with constant amplitude, constant average spin period (ω_0), and a variation period of approximately 365.2422 days. However, Telstar-401, Echostar-2, Solidaridad-1, and HGS-1 all appeared to have spin period variations with unique amplitudes and variation periods. Telstar-401's spin period variation (Fig. 12) was observed to have a period varying between 250 and 290 days. Echostar-2's and HGS-1's spin period variations (Fig. 14 and Fig. 16 respectively) were approximately one Earth orbit period. Solidaridad-1's spin period variation (Fig. 15) appeared to have a period (if periodic) of several years. However, the predicted behaviour of the spin angular acceleration over one variation period is roughly correct, considering that the angular accelerations of Telstar-401 (Fig. 19),

Echostar-2 (Fig. 21), Solidaridad-1 (Fig. 22), and HGS-1 (Fig. 23) appeared to be positive for approximately half of the variation period and negative for the remaining half.

Varying Solar Incidence Angles on Solar Panels

The maximum net angular acceleration estimated with Eq. 5 assumed that the solar incidence vector and the RSO spin axis vector were orthogonal and that the sunlight incidence angle on a solar panel would be 0° at one instance during a spin. If the scenario depicted in Fig. 31 is correct, Eq. 5 would not be valid.

If an RSO's spin axis direction is assumed to be fixed in inertial space and within Earth's equatorial plane (as shown in Fig. 31), then as the RSO spins, four solar panel normals (two normals corresponding to both sides of a single solar panel) would be tracing out great circles in equatorial inertial space, as shown for one panel in Fig. 32. In Fig. 32, \hat{n} is the normal of the sunlit panel side, $-\hat{n}$ is the normal of the opposite (unlit) panel side, α_{sun} and δ_{sun} are the equatorial coordinates of the Sun viewed from the Earth, α_{panel} and δ_{panel} are the instantaneous equatorial coordinates of \hat{n} , and γ is the instantaneous angle between \hat{n} and the Sun. The instantaneous coordinates of $-\hat{n}$ will be π radians apart in right ascension, and opposite in sign in declination, of \hat{n} , as shown in Fig. 32.

The Sun's equatorial coordinates, as viewed from the Earth, was estimated with Eq. 7 (right ascension) and Eq. 8. (declination), where ϵ is the obliquity of the ecliptic plane ($23^\circ.44$), and θ_{sun} is the ecliptic longitude of the Sun since the Vernal Equinox.

A solar panel normal's instantaneous equatorial coordinates, assuming the RSO orientation shown in Fig. 28 and assuming canted solar panels, was determined with Eq. 9 (right ascension) and Eq. 10 (declination). In Eq. 9 and Eq. 10, μ is the sidereal spin angle measured from the initial RSO orientation shown in Fig. 29.

The γ angle (ranging from 0° to 180°) was determined with Eq. 11. The cosine of the γ angle

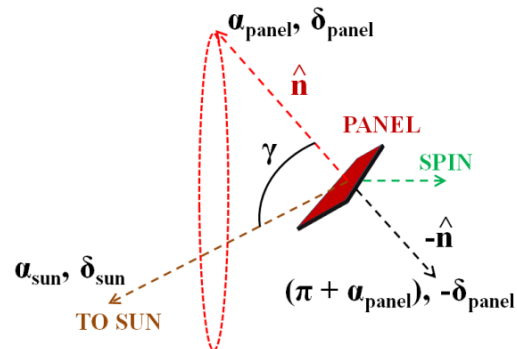


Fig. 32: Solar Geometry of a Single Panel Side

represents that component of the SRP that causes the RSO's angular acceleration. However, this angular acceleration will work to change both the spin period and the spin axis orientation, possibly causing spin axis precession. A solar panel side is illuminated when the γ angle is less than 90° .

$$\tan(\alpha_{sun}) = \cos(\epsilon) \tan(\theta_{sun}) \quad (7)$$

$$\cos(\delta_{sun}) = \frac{\cos(\theta_{sun})}{\cos(\alpha_{sun})} \quad (8)$$

$$\tan(\alpha_{panel}) = -\frac{\tan(\frac{\phi}{2})}{\cos(\mu)} \quad (9)$$

$$\cos(\delta_{panel}) = \frac{\cos(\mu)\cos(\frac{\phi}{2})}{\cos(\alpha_{panel})} \quad (10)$$

$$\cos(\gamma) = \sin(\delta_{sun}) \sin(\delta_{panel}) + \cos(\delta_{sun}) \cos(\delta_{panel}) \cos(\alpha_{sun} - \alpha_{panel}) \quad (11)$$

The total net SRP angular acceleration on a single solar panel side for one complete spin over an entire year was simulated. The result is shown in Fig. 33. A single solar panel side will either assist or oppose the RSO's spin depending on the spin axis orientation. This is why the y-axis in Fig. 33 contains only negative values.

The solar longitude of 0 in Fig. 33 corresponds to the sunlight incidence on the red solar panel at t_0 in Fig. 31. When the solar longitude reaches 90° , the panel side resists the spin with the smallest angular acceleration magnitude. Between solar longitudes 210° and 330° , the angular acceleration magnitude slightly decreases then increases again. This behaviour appears similar to Telstar-401's and Echostar-2's bumps shown in Fig. 23 and Fig. 25, respectively.

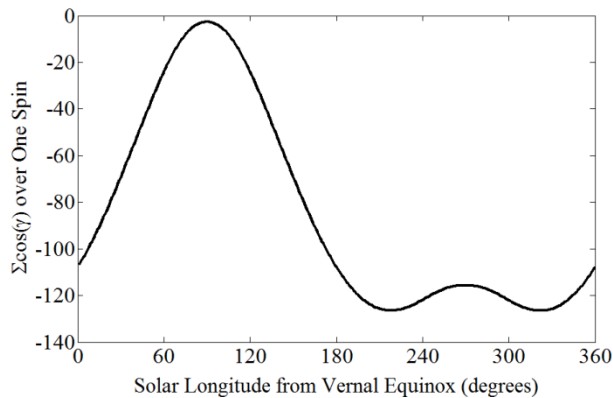


Fig. 33: Simulated Total Net Angular Acceleration from One Solar Panel Side over One Spin over an Earth Orbit

IV. CONCLUSIONS

The light curves pertaining to the six inactive box-wing GEO RSOs revealed that these RSOs were all spinning with unique spin periods. The spin periods were observed to vary in time, each with a unique rate and amplitude. In the cases of Telstar-401, Paksat-1, Echostar-2, Solidaridad-1, and HGS-1, the spin period variations were observed to have cyclical properties but with significantly different variation periods.

Telstar-401's, Echostar-2's and Solidaridad-1's spin period variations included decreasing angular acceleration magnitudes (bumps) near times when the observed angular acceleration magnitude was at maximum.

The most likely torque causing the observed angular accelerations was determined to be SRP. The maximum possible SRP torque was found to provide a potential angular acceleration several thousand times greater than those inferred to be acting on the RSOs.

The minimum absolute reflectivity difference between solar panel sides that could result in the observed maximum angular acceleration magnitudes was determined to be in the order of 10^{-4} . This demonstrated that nearly any reflectivity difference between any of the solar panels sides will result in a net SRP torque.

The synodic effect on a GEO RSO will be more pronounced for longer spin period RSOs and reflecting surface normals that are in close proximity to the spin axis during detected reflections.

As the Earth orbits the Sun, a GEO RSO with canted solar panels will encounter varying sunlight incidence angles that will change the net SRP torque and net angular acceleration magnitudes over the year. Assuming a fixed RSO spin axis in inertial space, this effect will be cyclical with a period of a sidereal year.

V. DISCUSSION

This paper has provided an explanation of hypotheses considered when studying inactive box-wing GEO RSOs' attitude dynamics. The most important part of this paper is the RSO observations because no hypothesis or simulation can be verified without them. The RSO observations referred to in this paper signify the first long-term high frequency survey of inactive box-wing GEO RSO spin periods to be published. However, these observations are far from complete, despite the knowledge that has been gained thus far.

At present, it is unknown whether or not the observed RSO spin periods contain significant synodic effects. If synodic effects are present, then the effort to separate the real components (SRP torque) from the virtual (synodic) will become more difficult and would

require months, if not years, of very careful observations of each RSO.

The apparent relationship between the spin period variation amplitude and the average spin period could provide a method of determining the approximate spin period variation characteristics from only a few observations of the RSO spin period. The apparent relationship might not be as linear as this paper implies.

The RSOs' MOI uncertainties would be greatly reduced once more accurate RSO specifications, specifically dimensions and component masses, are available. At present, the only sources of this information are the major American satellite contracting companies (Hughes, Lockheed Martin, and Boeing), and possibly some of the subcontractors.

Preliminary modelling of the sunlight variations on the RSO solar panels was an initial effort to understand the physics behind the RSOs' attitude dynamics. At present, the best hypothesis that could explain the majority of the observed spin period variations is the constantly varying effects of SRP torque as the Earth orbits the Sun.

VI. FUTURE WORK

The most important effort with respect to this research is the continuation of the RSO observations for another several years. As part of his PhD thesis, the primary author will be observing 20 inactive box-wing GEO RSOs and several GEO RSOs without large solar panels for comparison.

More detailed and accurate RSO specifications will be sought in the near future to improve the MOI accuracy. This effort could also improve the knowledge of each RSO's spin axis location and orientation.

Analytical, empirical and numerical box-wing RSO attitude dynamics modelling based on rigid body dynamics will commence in early 2015. This work will focus on SRP torques acting on spinning spacecraft with large solar panels, attitude dynamics, and possible synodic effects.

VII. ACKNOWLEDGMENTS

The primary author wishes to acknowledge the support and efforts of Lt. Col. Phil Somers (retd.), Dr. Gregg A. Wade (co-author), the Canadian Director General Space (DG Space), Defence Research and Development Canada (DRDC) and Ms. Jane E. Yaeger.

REFERENCES

[1] Mark Wade. Encyclopedia Astronautica. <http://www.astronautix.com>, 2011.

[2] P. Papishev, Yu. Karavaev, and M. Mishina. Investigations of the evolution of optical characteristics and dynamics of proper rotation of uncontrolled geostationary artificial satellites. *Advances in Space Research*, Vol. 43: pp. 1416–1422, 2009.

[3] D. Chu, S. Chen, D. Early, D. Freesland, A. Krimchansky, B. Naasz, A. Reth, K. Tadikonda, J. Tsui, and T. Walsh. GOES-R Stationkeeping and Momentum Management. *Proceedings of the 29th Annual AAS Rocky Mountain Guidance and Control Conference*, Vol. 125, pp. 277-291, 2006.

[4] C. Früh, and T Schildknecht. Attitude Motion of Space Debris Objects under Influence of Solar Radiation Pressure and Gravity. *Proceedings of the 63rd International Astronautical Congress, Naples, Italy*, IAC-12.A6.2.6, Vol. 3, pp. 2350-2355, 2012.

[5] J. Lambert, D. Hall, J. Africano, K. Kremeyer, and P. Kervin. Observations of Retired Boeing 376 Spacecraft. *Proceedings of the AMOS Technical Conference*, 2003.

[6] P. Somers. Cylindrical RSO Signatures, Spin Axis Orientation and Rotation Period Determination. *Proceedings of the AMOS Technical Conference*, 2011.

[7] US Strategic Command (USSTRATCOM). Space-Track. www.space-track.org, 2014.

[8] G. D. Krebs. Gunter's Space Page. <http://space.skyrocket.de>, 2012.

[9] B. Shoelson. *lombscargle.m* MATLAB Lomb-Scargle code. www.mathworks.com, 2011.

[10] J. R. Wertz. *Orbit & Constellation Design and Management*. Microcosm Press / Springer, 2009.